

Optimization of a moving sensor trajectory for observing a point scalar source in turbulent flow

Constantinos F. Panagiotou* and Davide Cerizza
*Institute of Industrial Science, The University of Tokyo,
Komaba 4-6-1, Meguro-ku, Tokyo 153-8505, Japan*

Tamer A. Zaki†
Department of Mechanical Engineering, Johns Hopkins University, Baltimore, MD 21218, USA

Yosuke Hasegawa‡
*Institute of Industrial Science, The University of Tokyo,
Komaba 4-6-1, Meguro-ku, Tokyo 153-8505, Japan*

(Dated: February 21, 2022)

We propose a strategy for optimizing a sensor trajectory in order to estimate the time dependence of a localized scalar source in a turbulent environment. We develop and test the algorithm in turbulent channel flow. The approach leverages the view of the adjoint scalar field as the sensitivity of measurement to a possible source. A cost functional is constructed so that the optimal sensor trajectory maintains a high sensitivity and low temporal variation in the measured signal, for a given source location. This naturally leads to the adjoint-of-adjoint equation based on which the sensor trajectory is iteratively optimized. It is shown that the estimation accuracy based on the measurement from a sensor moving along the optimal trajectory is drastically improved from that achieved with a stationary sensor. It is also shown that the ratio of the fluctuation and the mean of the sensitivity for a given sensor trajectory can be used as a diagnostic tool to evaluate the resulting performance. Based on this finding, we propose a new cost functional which only includes the ratio without any adjustable parameters, and demonstrate its effectiveness in predicting the time dependence of scalar release from the source.

I. INTRODUCTION

It is well known that animals and insects heavily rely on their advanced olfactory sense for a variety of activities, such as food scavenging, mating and avoiding predators. As a result, humans use the superior sensitivity of animals in various applications. For example, dogs have been extensively used for drug identification and search and rescue operations. Concurrently, the rapid advancements in robotics and sensory systems suggest that mobile robots or vehicles could successfully replace animals. Such technologies should be particularly important for operations under hazardous environments which are inaccessible to humans or animals. In order to achieve these goals, the development of efficient algorithms for characterizing a scalar source based on limited sensor signals in a turbulent environment is important [1, 2].

Existing algorithms for scalar source identification can be classified into two categories: reactive and model-based algorithms. The former prescribes sensor movement based on a sensor signal. In such a strategy, the flow environment is treated as a black box, and the algorithms for sensor movement are often inspired by the motions of biological organisms [3–5]. In contrast, the latter explicitly takes into account the mathematical models of fluid flow and associated scalar transport. Although the computational cost for the latter tends to become higher, a model-based method is expected to show superior performance than a reactive one, since complex dynamics of scalar transport are incorporated in their algorithms. However, their superiority has not been fully verified yet [6].

The model-based approaches generally result in an optimization problem, in which minimization of a cost functional is required under some constraints. Optimization techniques can generally be categorized into probabilistic [7–11] and deterministic methods [12–14]. Probabilistic approaches explore a parameter space in a probabilistic way until they reach the global optimum. For example, the infotaxis strategy developed by Vergassola *et al.* [15] is based on the Bayesian inference and seeks to minimize the Shannon entropy in order to locate the scalar source. Keats *et al.* [16] proposed a computationally efficient algorithm by combining the adjoint advection-diffusion equation with Monte Carlo Markov Chain sampling to evaluate the posterior probability. Although probabilistic approaches are effective

* corresponding author: co.panayiotou@cut.ac.cy

† t.zaki@jhu.edu

‡ ysk@iis.u-tokyo.ac.jp

in relatively simple flow configurations, it is not feasible to extend them to unsteady and three-dimensional flow environments, where the degrees of freedom of the design parameters drastically increase. For example, the algorithm proposed by Keats *et al.* [16] requires to solve the adjoint equation for each sensor, so that its computational cost increases with a number of sensors.

In the deterministic methods, the set of design parameters are simultaneously optimized based on the associated gradients of a prescribed cost functional. Their unique feature is that the computational cost does not depend on the number of design parameters, although a resultant solution may reach a local optimum. Cerizza *et al.* [17] developed a deterministic method for estimating the time history of the scalar source intensity at a known source location in a fully developed turbulent channel flow reproduced by direct numerical simulation (DNS). A finite number of stationary sensors were placed in the downstream of the scalar source, and the temporal change of the scalar source intensity was estimated from the downstream sensor signals by applying the adjoint analysis. Using a similar approach, Wang *et al.* [18] reconstructed the spatial location of the source from remote measurements. In both studies, a scalar source distribution is estimated by solving the adjoint scalar field, which can be interpreted as the sensitivity of a sensor [16].

The adjoint advection-diffusion equation has a source term at the sensor location, and it is solved backward in time with a negative advection velocity. Consequently, the resultant adjoint scalar field propagates upstream towards possible sources in the past. It can be shown that iterative update of an estimated scalar source based on the adjoint scalar field guarantees a monotonic decrease in the squared error between the true and estimated scalar concentration at a sensor location [17]. Cerizza *et al.* [17] systematically changed the streamwise distance between a scalar source and a sensor, and reported the impact on the estimation performance at different pulsation frequencies of the source. They also showed that the estimation performance is drastically improved with increasing the number of sensors. This suggests that the adjoint scalar fields generated at different sensor locations have complementary effects, so that the overall sensor sensitivity at the source location is enhanced.

Although Cerizza *et al.* [17] assumed sensors are stationary, it is expected that higher estimation performance could also be achieved by moving a single sensor along a proper trajectory without increasing the number of sensors. Indeed, there exist several studies for optimizing sensor arrangement and trajectory. In the field of meteorology, the impacts of sensor measurements on the forecast error have been considered in the framework of static 3D-variational [19, 20] and 4D-variational methods [21]. The obtained sensitivity information of measurements can be used to decide a next sensor location or optimize sensor arrangement [21, 22]. However, these approaches assume that the grand truth is known, and also require to solve a second-order adjoint problem, so that a computational cost tends to be large. In order to overcome the above issues, Kang and Xu [23] extended the concept of unobservability proposed by Krener and Ide [24], and considered the sensitivity of measurements on control variables, e.g., an initial condition in the case of 4D variational method. In this framework, a certain sensor arrangement is considered to be better, if possible changes of control variables could have larger impacts on measurements. This allows to quantitatively evaluate a given sensor arrangement without the information on the grand truth. Later, Mons *et al.* [25] applied optimal control theory to optimization of sensor arrangement for estimating a two-dimensional flow past a rotationally oscillating cylinder. A key feature of the latter study is that the adjoint-of-the-adjoint equation is derived for maximizing the observability, and this opens up a possibility of dealing with control variables with large degrees of freedom. In the field of informatics, a similar idea of maximizing the sensor sensitivity on control variables has been proposed by considering Fisher information matrix, and applied to optimization of the trajectories of mobile sensors [26, 27]. However, its application is limited to relatively simple problems such as a steady two-dimensional diffusion equation, and also control variables with limited degrees of freedom.

More recently, data-driven approaches have also been proposed for optimizing sensor arrangement. Verma *et al.* [28] considered optimization problem of the arrangement of shear-stress and pressure sensors around an artificial swimmer to identify the location and the oscillation mode of a nearby object. They define a utility function which quantify the independence of sensor signals resulting from the object and its movement, and the sensor locations are optimized so as to maximize the utility function. Deng *et al.* [29] developed a strategy for finding minimum sensor locations for identifying the Reynolds-averaged Navier-Stokes (RANS) model constants. Mons *et al.* [11] applied a Kriging-enhanced ensemble variational technique for scalar source estimation, and obtained the optimal arrangement of multiple stationary sensors by maximizing the condition number of a matrix describing the source-sensor relationship. Although these approaches have potential for wide applicability, they commonly require a number of simulations for possible sources (or control variables) before the fact, and therefore could be effective only in the cases where the search domain for control variables is confined.

In the present study, we extend the approach based on the sensor sensitivity considered in Kang and Xu [23], Mons *et al.* [25] to trajectory optimization of a moving sensor for observing a point scalar source in a fully developed turbulent channel flow. For this purpose, we revisit the physical meaning of the adjoint scalar field as the sensitivity of measurement, and formulate the problem as optimization of the sensitivity of a moving sensor for a given source location. This naturally leads to an extra-adjoint equation, or the adjoint-of-the-adjoint, based on which the sensor trajectory can be optimized. We show that not only the intensity of the sensor sensitivity, but also its uniformity

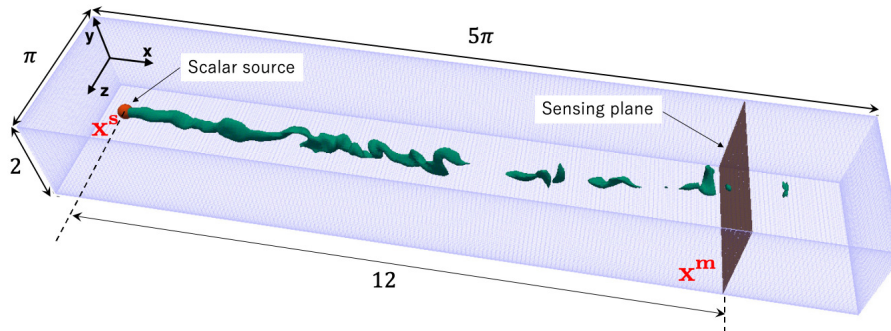


FIG. 1: Schematic of the computational domain.

within the search domain is crucial for better reconstruction of the scalar source. We propose a new cost functional for optimizing the trajectory of a moving sensor, and demonstrate that the obtained sensor trajectory results in an estimation performance as high as those obtained by seventeen stationary sensors.

The current paper proceeds as follows: After describing the flow configurations and the numerical scheme in § 2, we briefly introduce the estimation results of stationary sensors in § 3. In § 4, we develop an optimization strategy for a moving sensor trajectory. Then, the estimation performances of a moving sensor are presented and compared with those by single and multiple stationary sensors in § 5. Summary and conclusions of the present study are given in § 6.

II. COMPUTATIONAL SETUP

We consider a statistically stationary turbulent channel flow, in which a passive scalar is released from a stationary point source. Throughout this work, all variables are non-dimensionalized by the friction velocity u_τ and the half height of the channel h , unless otherwise stated. Figure 1 shows the computational domain and the coordinate system, where the streamwise, wall-normal and spanwise coordinates are denoted by x , y , z respectively. The dimensions of the computational domain along the streamwise and spanwise directions are set to be 5π and π , respectively. The origin of the coordinate system is located at the channel center, so that $y = -1$ and 1 correspond to the locations of the bottom and top walls, respectively. Throughout this study, the position of the scalar source, denoted as x_i^s , is located at the centerline of the channel, so that $(x^s, y^s, z^s) = (1.0, 0, \pi/2)$. We assume that the scalar source location is given, while the time history of the scalar source intensity is unknown. Hence, our goal is to estimate the scalar source intensity based on the sensor measurement downstream.

The problem design is intended to mimic a hazardous environment where the moving sensor can not approach the source, and is hence restricted in its motion. The position of a moving sensor is denoted by $x_i^m(t)$ which is in general an arbitrary function of time t . In the present study, the sensor is assumed to move freely in the y - z plane, while its x -coordinate is fixed to $x_1^m = 13.0$. This way, the estimation performances obtained from stationary and moving sensors will be compared under the same streamwise separation of $L_x = 12$ between the source and the sensors. Hereafter, the x -plane where the sensor is located is referred to as a sensing plane.

We assume an incompressible and Newtonian fluid, so that its governing equations are given by the following momentum and continuity equations:

$$\frac{\partial u_i}{\partial t} + u_j \frac{\partial u_i}{\partial x_j} = -\frac{\partial p}{\partial x_i} + \frac{1}{Re_\tau} \frac{\partial^2 u_i}{\partial x_j^2}, \quad (1)$$

$$\frac{\partial u_j}{\partial x_j} = 0, \quad (2)$$

where u_i is the velocity component in the i -th direction and p is the static pressure. The flow is driven by a constant mean pressure gradient imposed along the streamwise direction x , and the friction Reynolds number is defined as $Re_\tau = \frac{u_\tau h}{\nu} = 150$, where ν is the kinematic viscosity. This corresponds to the bulk Reynolds number of $Re_b \equiv U_b h / \nu \approx 2300$, where U_b is the bulk mean velocity. No-slip boundary conditions are imposed at the top and bottom walls, while periodic conditions are applied in the x and z directions.

The transport equation of a passive scalar c is given by

$$\frac{\partial c}{\partial t} + u_j \frac{\partial c}{\partial x_j} = \frac{1}{Pe} \frac{\partial^2 c}{\partial x_j^2} + Q(\mathbf{x}, t), \quad (3)$$

where $Q(\mathbf{x}, t)$ is a scalar source, which can be considered as an arbitrary function of space and time. The Peclet number is defined as $Pe = \frac{u_\tau h}{\Gamma}$, while Γ is the coefficient of mass diffusivity of the scalar. In the present study, the Peclet number is chosen to be equal to Re_τ , so that the Schmidt number $Sc = Pe/Re_\tau = \nu/\Gamma$ is unity.

Assuming the scalar source is spatially localized and its intensity changes in time as $\phi(t)$, the scalar source can be represented by

$$Q(\mathbf{x}, t) = \phi(t)\delta(\mathbf{x} - \mathbf{x}^s), \quad (4)$$

where δ is the Dirac's delta function. In the current study, we approximate the delta function with a steep Gaussian function in order to avoid numerical oscillation,

$$\delta(\mathbf{x} - \mathbf{x}^s) \simeq \left(\frac{\beta}{\pi}\right)^{3/2} \exp(-\beta|\mathbf{x} - \mathbf{x}^s|^2), \quad (5)$$

where β is chosen so that the scalar source is distributed over several grid points. The temporal part of the source function $\phi(t)$ is set as

$$\phi(t) = \frac{1}{2} \left\{ 1 + \cos(2\pi ft + \pi) \right\}, \quad (6)$$

so that it smoothly changes between 0 and 1 at a single frequency f . The initial and boundary conditions for the scalar field are given as

$$c(\mathbf{x}, t = 0) = 0, \forall \mathbf{x} \in \Omega \quad (7a)$$

$$\frac{\partial c}{\partial x_j} n_j = 0 \quad \text{at } y = \pm 1, \quad (7b)$$

where n_j represents the outward normal vector on the wall boundary and Ω refers to the entire fluid domain. In addition, we remove the scalar in the proximity of the domain boundaries along the streamwise and spanwise directions in order to avoid the scalar entering from the opposite side by virtue of the periodic conditions

Direct numerical simulation is adopted for solving the velocity and scalar equations. For spatial discretization, we use a pseudo-spectral method, where Fourier expansion is adopted in the x and z directions, while Chebyshev polynomials are used in the y direction. The code has been validated and applied to control and estimation problems in previous studies [30, 31]. The numbers of modes are set to be $(N_1, N_2, N_3) = (128, 65, 64)$ along the streamwise, wall-normal and spanwise directions, respectively. In order to remove aliasing errors, the 3/2 rule is employed, so that the numbers of the physical grid points are 1.5 times larger in all the directions. The present numerical scheme and condition are essentially identical to those in Cerizza *et al.* [17], where extensive verification of the present code is presented.

III. SCALAR SOURCE ESTIMATION BY STATIONARY SENSORS

In this section, we first summarize the fundamental mathematical properties of the adjoint scalar field, and discuss its physical interpretation from a viewpoint of scalar source estimation. Then, we will show that the adjoint scalar equation can be naturally derived by minimizing the squared error between the true and estimated scalar concentration at a sensor location. Finally, we present the estimation performances of stationary sensors. These results will provide us reference data to compare with those by a moving sensor in § 5.

A. Duality relationship

The adjoint scalar field c^* is defined so that it satisfies the following duality relationship:

$$\langle c^*, \mathcal{N}(c) \rangle = \langle \mathcal{N}^*(c^*), c \rangle + \mathcal{B}. \quad (8)$$

In equation (8), the bracket indicates the spatio-temporal integration, so that

$$\langle \cdot \rangle = \int_0^T \int_{\Omega} \cdot dV dt, \quad (9)$$

whereas \mathcal{N} and \mathcal{N}^* are an advection-diffusion operator and its adjoint, which are respectively defined as

$$\mathcal{N} = \frac{\partial}{\partial t} + u_j \frac{\partial}{\partial x_j} - \frac{1}{Pe} \frac{\partial^2}{\partial x_j^2}, \quad (10)$$

$$\mathcal{N}^* = -\frac{\partial}{\partial t} - u_j \frac{\partial}{\partial x_j} - \frac{1}{Pe} \frac{\partial^2}{\partial x_j^2}. \quad (11)$$

The second term on the right-hand-side of Eq. (8) is a boundary term defined as

$$\mathcal{B} = \left\langle \frac{\partial(cc^*)}{\partial t} + \frac{\partial}{\partial x_j} \left\{ c^* c u_j + \frac{1}{Pe} \left(c \frac{\partial c^*}{\partial x_j} - c^* \frac{\partial c}{\partial x_j} \right) \right\} \right\rangle. \quad (12)$$

Since the integrand has a divergence form, its spatio-temporal integration only depends on the values on the boundaries. In the present configuration, the boundary term becomes exactly zero, so that we will not consider it hereafter.

Substituting $\mathcal{N}(c) = Q$ and $\mathcal{N}^*(c^*) = \delta(\mathbf{x} - \mathbf{x}^m)\delta(t - t^m)$ into equation (8) yields

$$\langle c^*, Q \rangle = \langle \delta(\mathbf{x} - \mathbf{x}^m)\delta(t - t^m), c \rangle = c(\mathbf{x}^m, t^m) \equiv M(t^m). \quad (13)$$

This particular choices of $\mathcal{N}^*(c^*)$ is made, so that the right-hand-side of Eq. (13) is equal to the measurement signal $M(t^m)$, i.e., the concentration at sensor location \mathbf{x}^m and time t^m

Equation (13) indicates that the measurement signal can be evaluated in two ways: We can compute the forward evolution from a source Q and sample at the sensor. Alternatively, we can use the adjoint field c^* starting from a delta function at the sensor location, and perform dot product with the source Q . A higher value of c^* means higher contribution of Q at a particular location and time to the integral, thereby the sensor signal. This in turn provides physical interpretation of the adjoint field, that is, the sensitivity of the measurement.

In contrast to the forward operator (10) for the scalar field c , the adjoint scalar field has to be solved backward in time by using the advection velocity with an opposite sign as can be seen from Eq. (11). This is reasonable considering that a sensor signal at a certain location \mathbf{x}^m and time t^m should be caused by a scalar source present upstream at an earlier time.

B. Algorithm for scalar source estimation

In the adjoint-based estimation of scalar source, an arbitrary scalar source distribution in time and space is first assumed as an initial guess, and then it is iteratively optimized so as to minimize the error between the estimated scalar concentration and the measurement at sensor locations within a certain time horizon T . Hence, we introduce the following cost function J :

$$J = \int_0^T \frac{1}{2} \sum_k \left\{ c(\mathbf{x}_k^m, t) - M_k(t) \right\}^2 dt, \quad (14)$$

where $c(\mathbf{x}_k^m, t)$ is the estimated scalar concentration at the k -th sensor location, whereas $M_k(t)$ is the corresponding measurement. In the present study, the measurement noise is neglected, so that $M_k(t)$ is directly provided from the DNS results. The time horizon is set to be $T = 3$, which is normalized by the friction velocity and the channel half height. This is converted to $T^+ = 450$ in wall units. The corresponding convection distance $L_c^+ = U_b^+ \cdot T^+ \approx 6800$ is around three times the streamwise dimension of the computational box.

Minimizing J under the constraint of the scalar advection-diffusion equation is equivalent to minimizing the following Hamiltonian:

$$H = J - \langle c^* \{ \mathcal{N}(c) - \phi(t)\delta(\mathbf{x} - \mathbf{x}^s) \} \rangle, \quad (15)$$

where the adjoint scalar field c^* can be regarded as a Lagrange multiplier. In the present study, we assume a single point source at a known location \mathbf{x}^s . Hence, our problem is to estimate the temporal change of the source intensity $\phi(t)$.

By applying Fréchet differential to H with respect to $\phi(t)$ and integration by parts, we finally reach at the following expression (see, Cerizza *et al.* [17] for the details of the derivation):

$$H' \equiv \frac{\mathcal{D}H}{\mathcal{D}\phi} \phi' = \int_0^T c^*(\mathbf{x}^s, t) \phi'(t) dt, \quad (16)$$

where a variable with the prime indicates a perturbation caused by an infinitesimal change of ϕ . Here, the adjoint scalar field should satisfy the following equation

$$\begin{aligned} \mathcal{N}^*(c^*) &\equiv \left(\frac{\partial}{\partial t^*} - u_j \frac{\partial}{\partial x_j} - \frac{1}{Pe} \frac{\partial^2}{\partial x_j \partial x_j} \right) c^* \\ &= \sum_k \left\{ c(x_k^m, t) - M_k(t) \right\} \delta(\mathbf{x} - \mathbf{x}_k^m), \end{aligned} \quad (17)$$

under the following initial and boundary conditions:

$$c^*(\mathbf{x}, t^* = 0) = 0, \forall x \in \Omega, \quad (18a)$$

$$\frac{\partial c^*}{\partial x_j} n_j = 0 \text{ at } y = \pm 1, \quad (18b)$$

where the boundary conditions are periodicity in the spanwise z -direction, $c^* = 0$ at the inlet and outlet of the channel. In equation (17), $t^* = T - t$, so that t^* proceeds backward in the physical time t .

According to equation (16), the reduction of H is guaranteed when the source intensity is updated through the following expression:

$$\phi^{n+1}(t) = \phi^n(t) - \alpha c^*(\mathbf{x}^s, t), \quad (19)$$

where α is a constant and its optimal value is derived in Cerizza *et al.* [17]. For a detailed discussion regarding the method the reader should refer to the referenced work. It should be noted that the present algorithm can be applicable to a moving sensor by simply assuming that \mathbf{x}^m changes in time. In this case, the location of the source term in the adjoint equation (17) changes in time accordingly. The above algorithm will be used for estimating a scalar source intensity with a moving sensor in § 5.

C. Reference source reconstruction from stationary sensors

In this subsection, we revisit the problem of scalar-source reconstruction considered in Cerizza *et al.* [17] to get benchmark data, which will be used in § 5 as reference performance. Following Cerizza *et al.* [17], we placed stationary sensors downstream of the scalar source. Two different sensor placements are considered as shown in figure 2. In the first case, a single sensor is placed directly downstream of the scalar source. In the second case, seventeen sensors are distributed in the crossflow plane, surrounding the central sensor downstream of the scalar source, so that they will cover the mean scalar distribution in the sensing plane.

In figure 3, the time traces of the source intensity estimated from single and seventeen stationary sensors are plotted and compared with the true distribution, when the pulsating frequency of the source is set to be $f = 4$. As anticipated, employing seventeen sensors yields much better estimation than that of a single sensor. These results suggest that sensor arrangement plays a critical role in estimating a scalar source.

IV. STRATEGY FOR OPTIMIZING A SENSOR TRAJECTORY

A. Defining cost-functional

The better performance with seventeen stationary sensors shown in the previous section is due to their collective higher sensitivity to the scalar source location. This suggests that estimation performance could also be improved with a single sensor moving along an optimized trajectory, along which possible scalar releases at any instant can be captured by the moving sensor.

Suppose that a point scalar source at a location of \mathbf{x}^s instantaneously releases scalar at an arbitrary time t^s . Such an impulse scalar source may be modeled by $Q(\mathbf{x}, t) = \delta(\mathbf{x} - \mathbf{x}^s) \delta(t - t^s)$. If we assume continuous measurement in

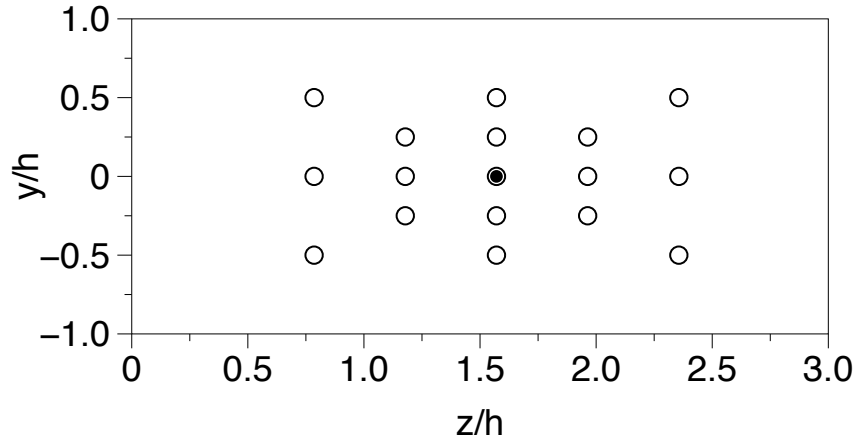


FIG. 2: Sensor arrangement in the y - z plane at $x = 13.1$. The open circles correspond to the locations of 17 sensors, whereas the filled circle indicates the location of a single sensor, which is placed at direct downstream of the source.

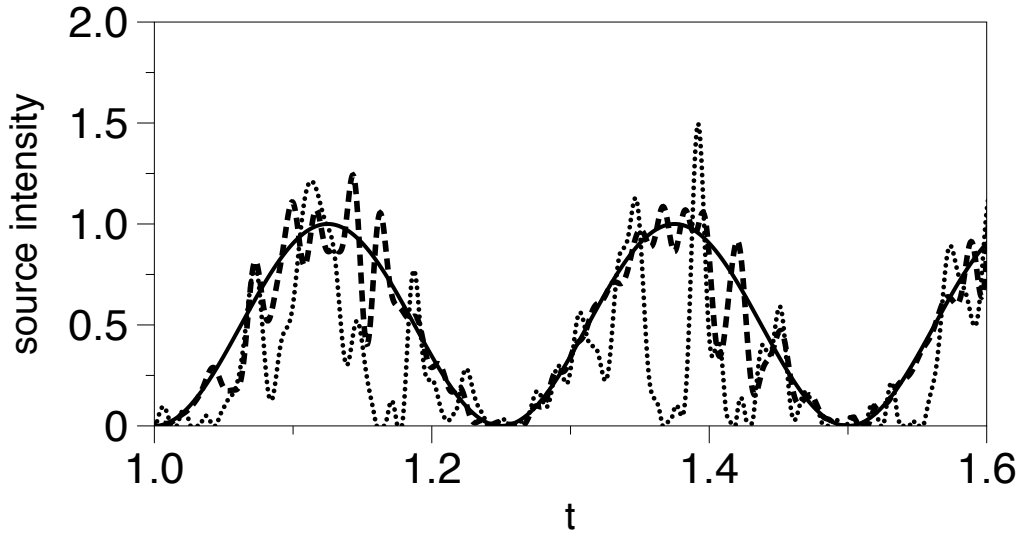


FIG. 3: Time trace of source intensity with pulsating frequency $f = 4$. solid line: true profile, dotted line: estimation with a single sensor, dashed line: estimation with seventeen sensors.

time at a sensor location \mathbf{x}^m , the time integral of the sensing signal caused by the impulse release can be obtained by substituting

$$\mathcal{N}^*(c^*) \equiv \frac{\partial c^*}{\partial t^*} - u_j \frac{\partial c^*}{\partial x_j} - \frac{1}{Pe} \frac{\partial^2 c^*}{\partial x_j \partial x_j} = \delta(\mathbf{x} - \mathbf{x}^m), \quad (20)$$

into the duality relationship (8). Note that, since we consider the time integral of the measurement signal, the delta function in time appeared in Eq. (13) is removed from $\mathcal{N}^*(c^*)$ here. Indeed, the above choice of $\mathcal{N}^*(c^*)$ leads to

$$\tilde{M} \equiv \int_{-\infty}^{\infty} M(t) dt = \langle c^*, \delta(\mathbf{x} - \mathbf{x}^s) \delta(t - t^s) \rangle = c^*(\mathbf{x}^s, t^s), \quad (21)$$

where a tilde represents an integral over time. The above equation indicates that the time integral of measurement at the sensor location \mathbf{x}^m can be given by the instantaneous adjoint scalar concentration at the source location \mathbf{x}^s and the instant of scalar release t^s .

Here, we make the following assumptions for better performance of scalar source estimation: First, when estimating scalar release from a source at a certain time t^s , the resultant time integral of the sensor signal should be high. Indeed,

if the scalar plume does not overlap the sensor location and there is no sensing signal, it is impossible to reconstruct the source. Second, the sensing signal resulting from an instantaneous scalar release within the time horizon should have similar intensity regardless of releasing time. If the sensor signal is weak for a particular releasing time, namely, the sensitivity of the sensor is low for the instantaneous scalar release, it becomes more difficult to accurately reconstruct the scalar source at the instant. For example, the source reconstruction with a single sensor presented in Fig. 3 shows large fluctuation, which may be attributed to the fluctuation of the sensitivity for instantaneous scalar release. It should be noted that the first assumption is similar to those adopted in Kang and Xu [23], Mons *et al.* [25], where the sensor arrangement is optimized so as to maximize the magnitude of the sensor sensitivity. Meanwhile, the second assumption, i.e., the uniformity of the sensitivity within the search domain, is newly introduced in the present study. As will be shown later, the second assumption further improves the estimation accuracy.

Based on the above considerations, we aim to maximize c^* at the source location with less fluctuation in time, and define the following cost functional to be minimized for finding the optimal sensor trajectory:

$$J_1 = -\alpha_1 \int_0^T c^*(\mathbf{x}^s, t) dt + \alpha_2 \int_0^T \left(c^*(\mathbf{x}^s, t) - \bar{c}^*(\mathbf{x}^s) \right)^2 dt + \alpha_3 \int_0^T \mathbf{u}^m \cdot \mathbf{u}^m dt, \quad (22)$$

where $\mathbf{u}^m = \frac{d\mathbf{x}^m}{dt}$ denotes the sensor velocity. The positive weighting constants α_1 , α_2 and α_3 are introduced in order to change the relative contribution from each term to J_1 . The first term contributes to increase the averaged sensitivity at the source location, while the second term tends to reduce its temporal fluctuation. The third term represents a penalty on the sensor speed, and works as a regularization term. The time horizon is set to $T = 3$, which is identical to that used for scalar source estimation from a stationary sensor in § 3.

B. Parameters for optimizing a sensor trajectory

In order to systematically change the contributions from the three terms in J_1 , we introduce the following two parameters.

The first one is

$$R_{21} = \frac{\alpha_2 \int_0^T \left[c^*(\mathbf{x}^s, t) - \bar{c}^*(\mathbf{x}^s) \right]^2 dt}{\alpha_1 \int_0^T c^*(\mathbf{x}^s, t) dt}, \quad (23)$$

which represents the ratio of the second and first terms in J_1 . The weighted constants α_1 and α_2 are determined so as to realize a prescribed value of R_{12} . A large value of R_{21} leads to a larger weight for the second term in J_1 suppressing the temporal fluctuation of c^* at the source location than the first term for maximizing the averaged value of c^* . The second parameter R_{31} corresponds to the ratio of the third and first terms of J_1 , and is defined as

$$R_{31} = \frac{\alpha_3 \int_0^T u_j^m u_j^m dt}{\alpha_1 \int_0^T c^*(\mathbf{x}^s, t) dt}. \quad (24)$$

Again, α_1 and α_3 will be adjusted so as to achieve a prescribed value of R_{31} .

Table I summarizes all combinations of R_{21} and R_{31} considered in the present study. In Case A, both R_{21} and R_{31} are null, so that only the first term of J_1 is taken into account. On the other hand, for cases B_1 - B_4 , the weight for the second term is systematically increased while the third term is kept zero. Finally, in case C, the effects of the third term are examined. Note that the time integrals in equations (23, 24) are in general unknown before optimizing a sensor trajectory. In the present study, their values are evaluated from the statistics of c^* for Case A, so that the values of α_1 , α_2 and α_3 are all fixed during the procedures of optimizing a sensor trajectory.

C. Performance indices

Once a sensor trajectory is successfully optimized in Cases B and C, it should reduce the temporal fluctuation of c^* with respect to its temporal average \bar{c}^* according to the definition of J_1 in equation (22). This motivates us to define the following ratio of the standard deviation and the time average of c^* at the source location:

$$\epsilon = \frac{\sqrt{\frac{1}{T} \int_0^T \left(c^*(\mathbf{x}^s, t) - \bar{c}^*(\mathbf{x}^s) \right)^2 dt}}{\frac{1}{T} \int_0^T c^*(\mathbf{x}^s, t) dt}, \quad (25)$$

Case	R_{21}	R_{31}	circular			random		
			ϵ	ψ^ϕ	ℓ_{norm}^2	ϵ	ψ^ϕ	ℓ_{norm}^2
A	0.0	0.0	1.23	0.74	0.29	1.10	0.80	0.25
B_1	0.1	0.0	1.18	0.76	0.27	1.06	0.82	0.24
B_2	1.0	0.0	0.94	0.77	0.26	0.85	0.89	0.17
B_3	10	0.0	1.30	0.55	0.39	1.17	0.58	0.36
B_4	∞	0.0	1.39	0.53	0.40	1.25	0.55	0.37
C	1.0	1.0	1.03	0.69	0.31	0.97	0.74	0.28
	initial		1.82	0.43	0.46	1.64	0.52	0.42

TABLE I: Summary of the numerical conditions and the resultant estimation performance.

which will be used to evaluate different sensor trajectories later.

As for a performance index of scalar source estimation, we define the correlation coefficient ψ^ϕ between the time traces of the true and estimated source intensities i.e., $\phi^{true}(t)$ and $\phi^{est}(t)$ as

$$\psi^\phi = \frac{\int_0^T (\phi^{true}(t) - \overline{\phi^{true}})(\phi^{est}(t) - \overline{\phi^{est}}) dt}{\sqrt{\int_0^T (\phi^{true}(t) - \overline{\phi^{true}})^2 dt} \sqrt{\int_0^T (\phi^{est}(t) - \overline{\phi^{est}})^2 dt}}. \quad (26)$$

Obviously, ψ^ϕ closer to unity indicates a better performance.

Another index is the L2 norm of the difference between $\phi^{true}(t)$ and $\phi^{est}(t)$, given by

$$\ell_{norm}^2 = \sqrt{\frac{1}{T} \int_0^T (\phi^{true}(t) - \phi^{est}(t))^2 dt}. \quad (27)$$

A smaller value of ℓ_{norm}^2 means a less estimation error, and thereby better estimation. In the following sections, ψ^ϕ and ℓ_{norm}^2 will be used to evaluate the estimation performances in all cases.

D. Derivation of optimization algorithm

Minimizing J_1 given by equation (22) requires optimization of the adjoint scalar field which is governed by equation (20). Hence, we define the following Hamiltonian for optimizing a sensor trajectory:

$$H = J_1 + \left\langle \theta \left\{ \frac{\partial c^*}{\partial t^*} - u_j \frac{\partial c^*}{\partial x_j} - \frac{1}{Pe} \frac{\partial^2 c^*}{\partial x_j \partial x_j} - \delta(\mathbf{x} - \mathbf{x}^m) \right\} \right\rangle, \quad (28)$$

where θ is a Lagrange multiplier, and can also be considered as the adjoint of the adjoint field. Our purpose is to optimize the sensor trajectory $\mathbf{x}^m(t)$ to minimize H . For this purpose, we can take a standard approach, which is essentially the same as equations (15)-(19) used for estimating scalar source. Namely, applying the Fréchet differential to equation (28) with respect to an infinitesimal change $(\mathbf{x}^m)'$ of a sensor trajectory, and integrating by parts (see, Appendix A for more details), we end up with

$$\begin{aligned} H' &\equiv \frac{\mathcal{D}H}{\mathcal{D}\mathbf{x}^m} (\mathbf{x}^m)' = \left\langle -\frac{\partial \theta}{\partial x_j} \delta(x_j - x_j^m) (x_j^m)' \right\rangle - 2\alpha_3 \int \frac{d^2 x_j^m}{dt^2} (x_j^m)' dt \\ &= \int_0^T - \left[\left(\frac{\partial \theta}{\partial x_j} \right)_{\mathbf{x}^m} + 2\alpha_3 \frac{d^2 x_j^m}{dt^2} \right] (x_j^m)' dt, \end{aligned} \quad (29)$$

where θ has to satisfy the following equation:

$$\frac{\partial \theta}{\partial t} + u_j \frac{\partial \theta}{\partial x_j} = \frac{1}{Pe} \frac{\partial^2 \theta}{\partial x_j^2} + \left\{ \alpha_1 - 2\alpha_2 (c^* - \overline{c^*}) \right\} \delta(\mathbf{x} - \mathbf{x}^s), \quad (30)$$

with the following initial and boundary conditions

$$\theta(\mathbf{x}, t = 0) = 0, \quad \forall \mathbf{x} \in \Omega \quad (31)$$

$$\frac{\partial \theta}{\partial x_j} n_j = 0, \quad \text{at } \partial\Omega. \quad (32)$$

Equation (29) indicates that H' is always negative if the sensor trajectory is updated based on the following expression:

$$(x_j^m)'(t) \equiv x_j^{m,n+1}(t) - x_j^{m,n}(t) = \alpha^n \left[\left(\frac{\partial \theta}{\partial x_j} \right)_{\mathbf{x}^m} + 2\alpha_3 \frac{d^2 x_j^m}{dt^2} \right]^n, \quad (33)$$

where the superscript n indicates the current iteration step and α is a positive coefficient determining the amount of the update in each iteration step.

Algorithm 1: Algorithm for optimizing sensor trajectory

- $n = 0$;
 - Solve equations (1, 2) and store all data regarding the velocity field;
 - Prescribe an initial guess of the sensor trajectory $\mathbf{x}^{m,0}$;
- while** *Convergence criterion is not satisfied* **do**
- Advance the adjoint equation $\mathcal{N}^*(c^*) = \delta(\mathbf{x} - \mathbf{x}^m)$ and record c^* at the source location to evaluate $\bar{c}^* = \frac{1}{T} \int_0^T c^*(\mathbf{x}^s, t) dt$;
 - Advance the adjoint-of-adjoint equation (30) for θ and store $\frac{\partial \theta}{\partial x_j}$ at sensor location for the entire time period;
 - Compute step size, $\alpha^n = 0.05 / \max \left| \left[\left(\frac{\partial \theta}{\partial x_j} \right)_{\mathbf{x}^m} + 2\alpha_3 \frac{d^2 x_j^m}{dt^2} \right]^n \right|$;
 - Update sensor's trajectory in accordance with equation (33);
 - $n = n + 1$
- end**
-

The overall procedure for optimizing a sensor trajectory is summarized in algorithm 1. First, we solve equations (1, 2) and store the spatio-temporal evolution of the entire velocity field within the computational domain Ω and the time horizon $0 \leq t \leq T$. This has to be done only once before starting optimization, and the same data set of the velocity field can be used throughout the following optimization procedures. Secondly, assuming an arbitrary initial sensor trajectory $\mathbf{x}^{m,0}$, the adjoint equation (20) is solved backward in time and c^* at the source location is recorded. Then, this information is used to solve the extra-adjoint equation (30) for θ . Note that, in contrast to equation (20), equation (30) is solved forward in the original time t . Once θ at the sensor location is obtained, the sensor trajectory is updated in accordance with equation (33). The above procedures are repeated until the sensor trajectory converges.

We considered two different initial trajectories which are both lying sufficiently close to the core of the plume at the measurement plane, so that a sensor receives significant signals. The first one is a circular motion, the center of which is located at the channel center and its radius is 0.2, and the second one is a trajectory generated by a random walk starting from the channel center. These two initial trajectories are depicted in figure 4, in which the iso-lines of the mean scalar concentration from the point source at \mathbf{x}^s with a steady release are also shown. It can be confirmed that both initial trajectories are within these contours.

V. RESULTS

We first show the optimal sensor trajectories obtained for Cases A-C in § 5.1. In § 5.2, the estimation performances based on the signals obtained from the optimal sensor trajectories are presented and compared with those of stationary sensors. Based on the obtained results, we propose a simpler and more effective strategy for optimizing a moving sensor trajectory, and validate its performance in § 5.3.

A. Optimal sensor trajectory

1. Cases A and B

First, we consider cases A and B, in which the penalty of the sensor velocity is neglected. Figure 5 shows the evolution of the cost functional convergence rate $\frac{\Delta J}{\Delta J_o} = \frac{J_1^n - J_1^{n-1}}{J_1^1 - J_1^0}$ as a function of a number of iterations. In the

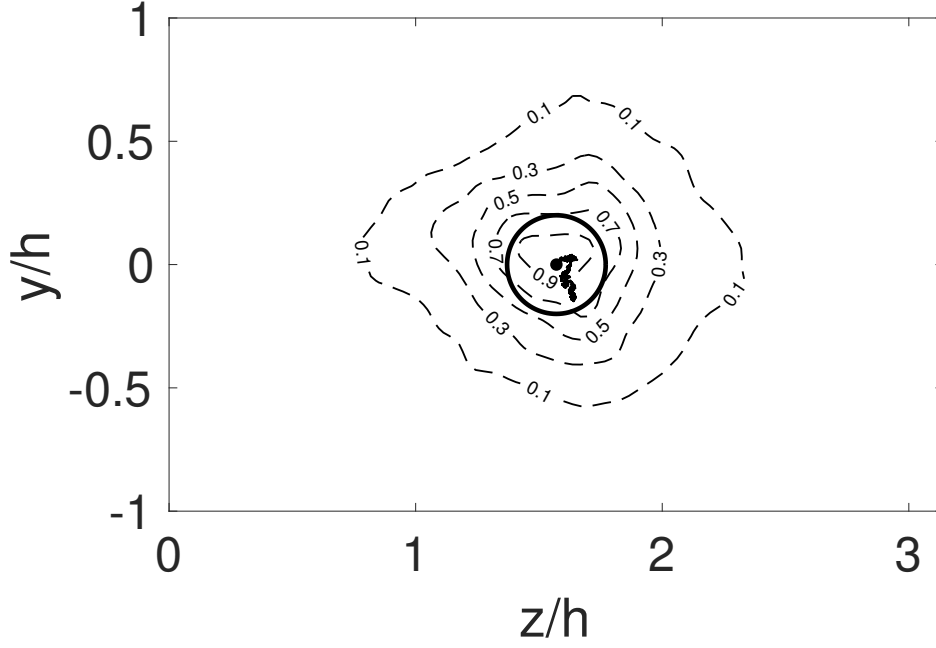


FIG. 4: Isolines of the averaged scalar field c at the y - z plane of motion, where the scalar field is time-averaged within the time interval $t \in (0, T)$. The values of the scalar field are normalized to the maximum averaged value. Solid lines indicate the initial sensor trajectories.

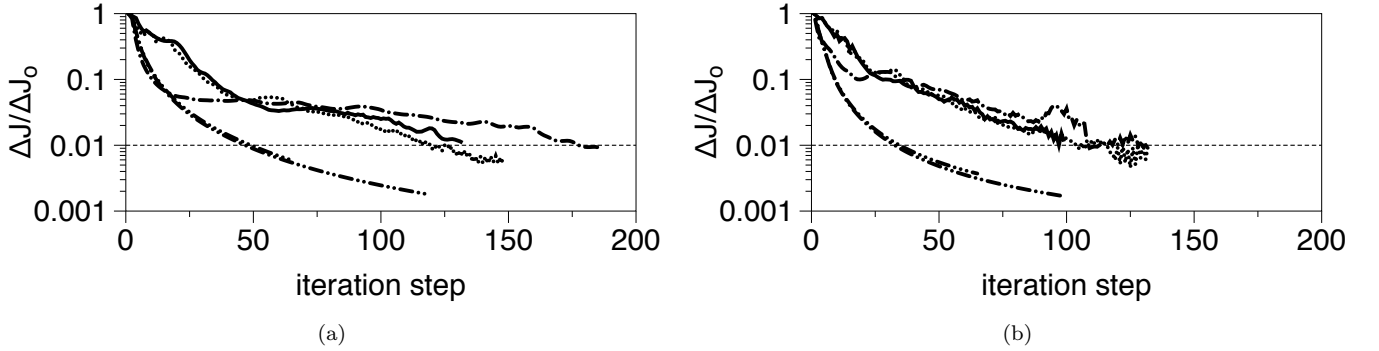


FIG. 5: Evolution of cost-functional convergence rate starting from (a) circular and (b) random trajectories. (—) $R_{21} = 0.0$; (.....) $R_{21} = 0.1$; (-·-·) $R_{21} = 1.0$; (- - - -) $R_{21} = 10.0$ (- - - -) $R_{21} \rightarrow \infty$. A thin horizontal lines corresponds to $\Delta J/\Delta J_0$ which is used to judge the convergence of each optimization.

current study, the iteration for optimizing a sensor trajectory is continued until the reduction of the cost functional becomes less than 1% of the initial update, which is depicted by a thin horizontal line.

Figure 6 shows the impact of R_{21} on the evolution of the cost functional (22) with the initial sensor trajectory generated by a random walk. Throughout the iterations, the first term in equation (22) is dominant for $R_{21} = 0.1$, whereas the second term becomes a primary factor for $R_{21} = 10$. These results indicate that the relative importance of the first and second terms in the cost functional (22) can be successfully controlled by changing R_{21} . Note that similar trends are also confirmed when the optimization is initiated from a circular trajectory (not shown here).

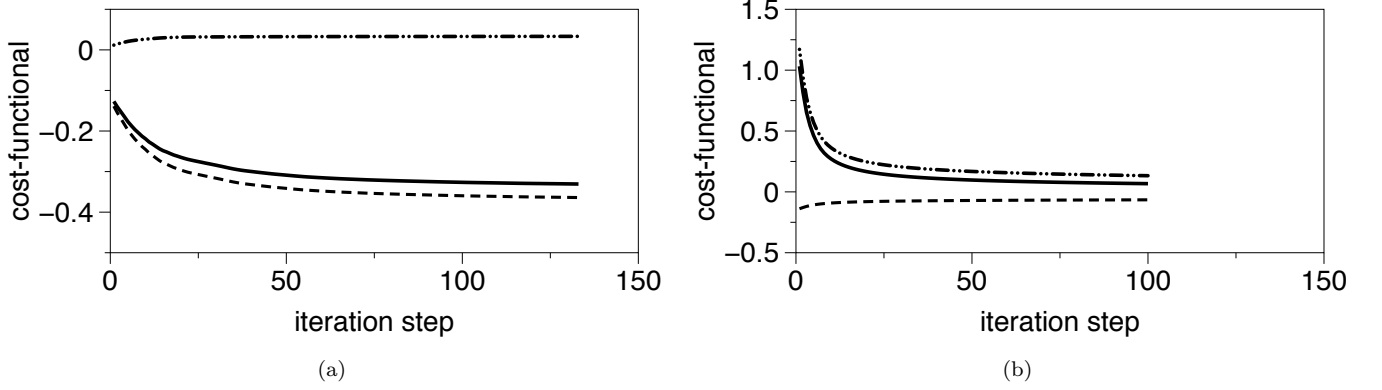


FIG. 6: Evolution of the total cost-functional and its individual components for (a) $R_{21} = 0.1$ and (b) $R_{21} = 10$, for an initially random trajectory. (—): the total cost-functional, (----): the first component, (-·-·-): the second component.

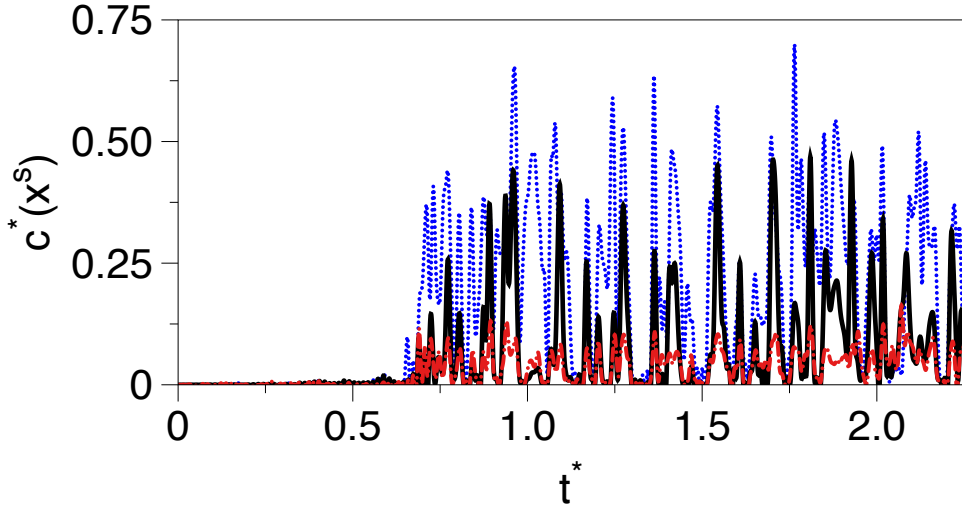


FIG. 7: Time trace of the adjoint field at the source location for an initially random trajectory. (—): the initial trajectory, (·····): $R_{21} = 0.1$, (-·-·-): $R_{21} = 10$.

Figure 7 shows the time trace of the adjoint field c^* at the source location obtained by the sensor trajectories optimized with different R_{21} from an initially random trajectory. Here, the horizontal axis is $t^* = T - t$, so that it proceeds backward in the original time t . It can be observed that c^* is absent during the initial period of $0 \leq t^* \leq 0.7$. This period corresponds to a time interval for the adjoint field generated at the sensor location reaches at the source location. Indeed, considering the advection velocity at the channel center is $u_c \approx 18$, and the streamwise distance between the sensor and the source is $L_x = 12$, the convection time is approximated as $T_c \approx L_x/u_c = 0.67$, which agrees well with the above initial period.

It is also found that the optimal sensor trajectories with large R_{21} suppress the fluctuation of c^* , whereas those with small values tends to increase the intensity of c^* with larger fluctuations. In order to quantify the fluctuation of c^* relative to its mean, ϵ defined in equation (25) is calculated and the results are listed for all cases in Table I. It is found that ϵ shows a non-monotonic relationship with R_{21} , and reaches its minimum at $R_{21} = 1$ regardless of the initial sensor trajectories. As will be shown later, large sensitivity with less fluctuation in time is a key for better estimation, and ϵ is generally correlated with the resultant estimation performance.

Figure 8 shows the time trace of the y -coordinate of the sensor trajectories optimized from random and circular ones.

It is found that a smaller R_{21} yields more spread sensor trajectory from the center line, i.e., $y = 0$, and quicker changes of sensor location, indicating high sensor velocity and abrupt changes in its sign. Furthermore, the correlation

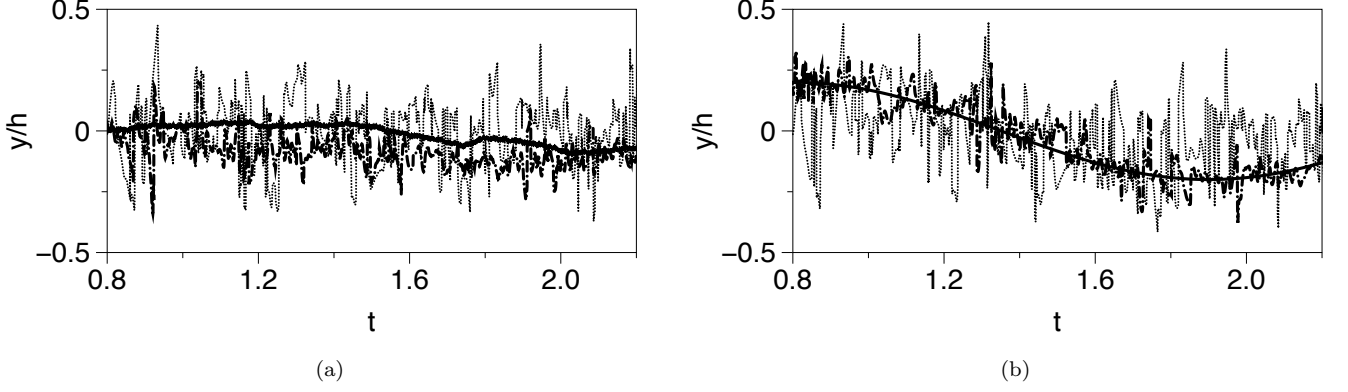


FIG. 8: Time trace of the sensor's trajectory along the y coordinate starting from (a) random and (b) circular trajectories. (—): the initial trajectory, (⋯): the optimal trajectory with $R_{21} = 0.1$, (— · —): the optimal trajectory with $R_{21} = 10$.

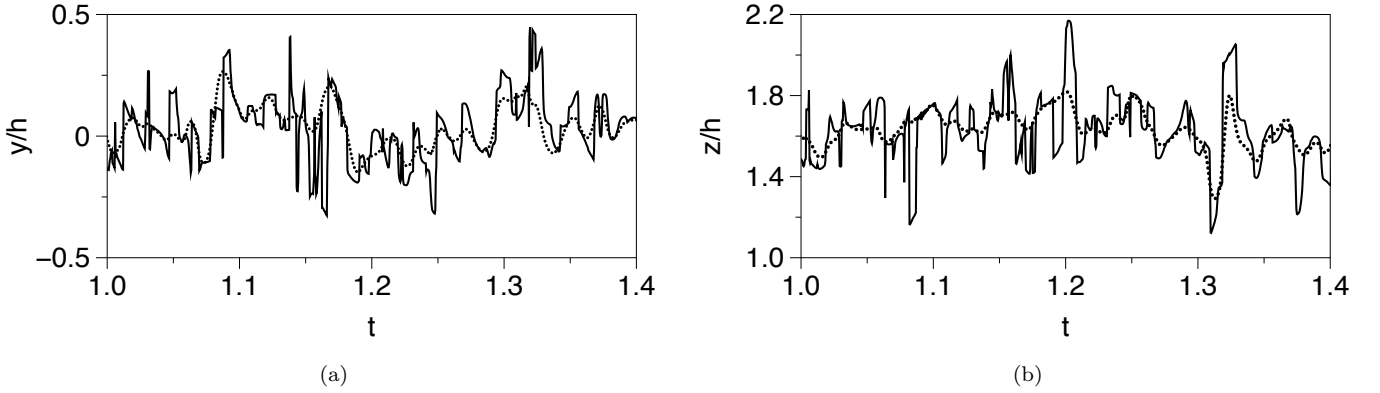


FIG. 9: Time traces of the (a) normal and (b) spanwise coordinate of the optimal sensor trajectory starting from a random trajectory. (—): Case B2 (⋯): Case C

coefficient between the optimal trajectories starting from circular and random trajectories is found to increase with decreasing value of R_{21} . The above observations could be explained by the source term appearing in the last term on the RHS of equation (30). For small R_{21} , this term tends to become constant, thus independent of sensor trajectory.

A similar trend is also observed for z coordinate of the sensor trajectory (not shown here).

2. Case C

Figure 9 shows the time traces of the sensor trajectories with and without the penalty of the sensor speed for Cases C and B2. It can be seen that non-zero value of R_{31} in Case C yields a smoother trajectory compared to $R_{31} = 0$ (Case B2). This is consistent with the presence of the penalty term, i.e., the third term in the cost functional (22).

Figures 10(a)-(b) show the time traces of the sensor speed for the two cases in the y and z directions, respectively. Here, the sensor speed is normalized by the bulk mean velocity \bar{u}_b . It is found that, for Case B2 where no penalization on the sensor velocity is imposed, the sensor velocity intermittently rises beyond the bulk mean velocity as shown by open circles in Figs. 10(a)-(b). In contrast, by introducing the penalization of the sensor velocity in Case C, the abrupt increase of the sensor velocity is suppressed, so that the sensor velocity is mostly below the bulk mean velocity.

Figure 11 shows the time traces of the adjoint fields at the source location which are generated from the optimal trajectories in Cases B2 and C. It is observed that the fluctuation of the adjoint field becomes larger in Case C, where the penalty of the sensor speed is introduced. This implies that the smoother sensor trajectory is obtained by

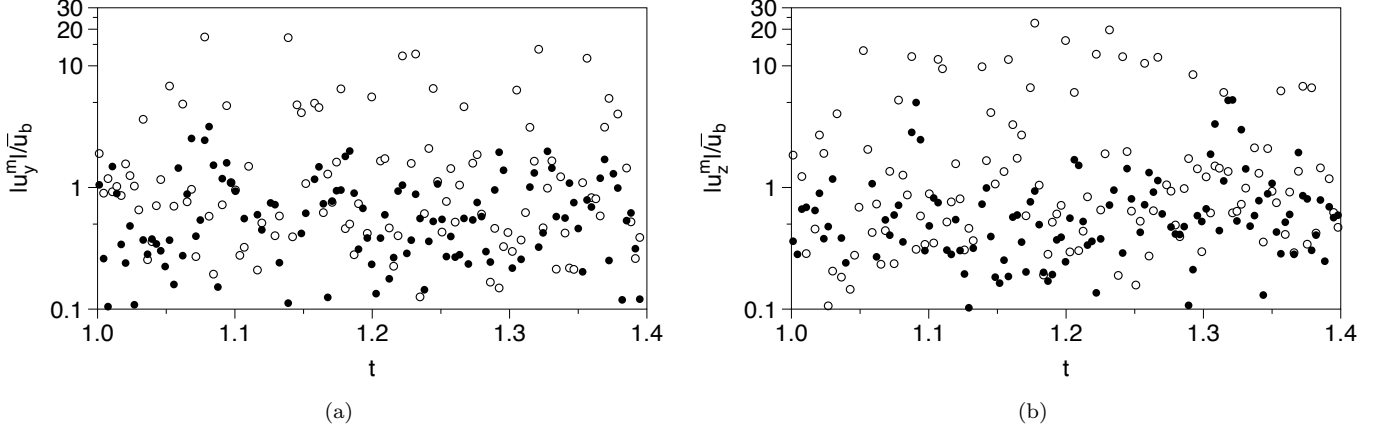


FIG. 10: *Top*: Time traces of sensor velocity along (a) wall-normal and (b) spanwise directions, normalized by the bulk mean velocity. Open and filled circles correspond to Cases *B2* and *C*, respectively.

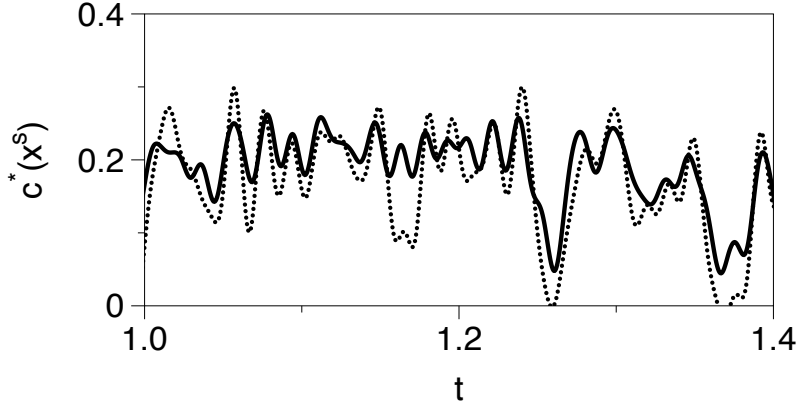


FIG. 11: Time trace of the adjoint field at the source location generated from the trajectories optimized from the initially random trajectory. — : Case *B2*, : Case *C*

compromising the stabilization of the temporal fluctuation of the adjoint field. This is also reflected to the increase of ϵ in Case *C* (see, Table I).

B. Scalar source estimation with optimal sensor trajectory

In the previous subsection, it was shown that the parameters R_{21} and R_{31} defined by equations (23, 24) successfully change the relative importance of the three terms comprising the cost functional (22), and the corresponding optimal sensor trajectories are obtained under the compromise of the three terms. Here, we evaluate the performances of scalar source reconstruction based on the signals obtained from the optimal trajectories.

Table I summarizes the reconstruction performances evaluated by the correlation coefficient ψ^ϕ and the L2 norm ℓ^2 . It is found that the optimal trajectories generally perform much better than the initial circular/random trajectory, and also the single stationary sensor. It should be also noted that the highest performance is commonly obtained in Case *B2* regardless of the initial sensor trajectory.

In figure 12, the true and estimated scalar source intensities are plotted. Consistent with Table I, the estimation with the optimal trajectory in Case *B2* shows the best match with the true profile. In order to explain the best estimation performance in Case *B2*, the adjoint scalar field at the source location for the initial random trajectory and the optimal trajectory are compared in the top figure of figure 13, whereas the resultant reconstruction of the scalar source is shown in the bottom. It can be seen that the estimation error is strongly correlated with the fluctuation of the adjoint field at the source location. A larger fluctuation generally causes a large deviation of the estimation from

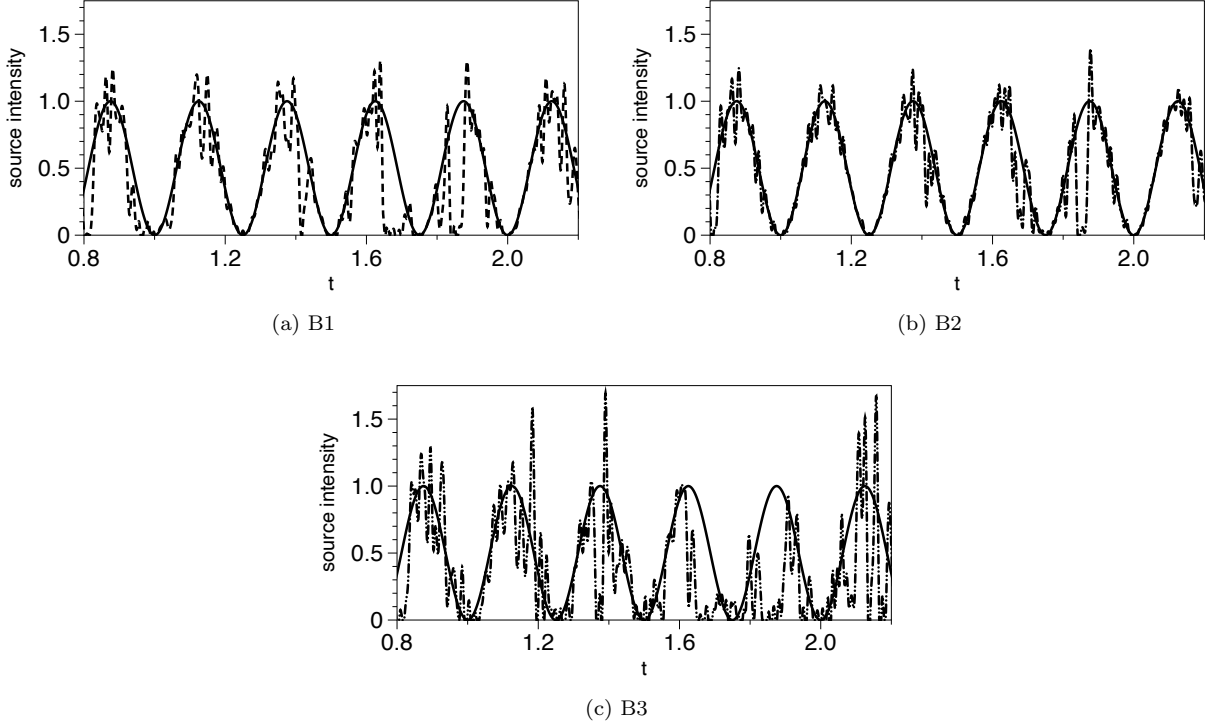


FIG. 12: Time traces of the source intensity estimated with trajectories optimized from the initial random trajectory. Solid line (—): true profile, dotted line (.....): Case B1, dashed dotted line (— · —): Case B2, dashed double dotted line (— · · —): Case B3. Only a limited time frame of the entire time horizon considered is shown.

the true profile. Especially, the presence of time periods with no significant adjoint field in the initial trajectory results in the failure of estimation during these periods. These results justify the current setting of the cost functional (22) and also suggest that ϵ can be used as a diagnostic parameter for the estimation capability. Indeed, as shown in Table I, the estimation performance is negatively correlated with ϵ .

We also address the effects of the penalty of the sensor speed on the estimation performance. As shown in figure 11, the adjoint field at the source location in Case C shows larger fluctuation than that in Case B2. As a result, ϵ is increased and the estimation performance is deteriorated (see, Table I). Adding the penalty term in the cost functional (22) results in a smoother trajectory at the cost of larger fluctuation of the adjoint field at the source location. This explains the worse performance in Case C.

C. Cost functional with ϵ

One of the main issues in the cost functional (22) is that it requires to find the optimal values of the weighting coefficients, i.e., R_{21} and R_{31} . Especially, the value of R_{21} is important to determine the relative importance of the first and second terms in equation (22). According to the present results, however, the estimation performance is well correlated with a single quantity, i.e., ϵ , throughout all the cases considered. This motivates us to define the following cost functional:

$$J_2 = \epsilon = \frac{c_{rms}^*(\mathbf{x}^s)}{c^*(\mathbf{x}^s)}. \quad (34)$$

The advantage of introducing the above cost functional is that there is no adjustable parameter.

Following the same procedure as described in § IVD, we obtain the following adjoint-of-the-adjoint equation for θ (see Appendix B for the detailed derivation):

$$\frac{\partial \theta}{\partial t} + \frac{\partial(\theta u_j)}{\partial x_j} = \left\{ \frac{\partial}{\partial x_j} \left(\frac{1}{Pe} \frac{\partial \theta}{\partial x_j} \right) \right\} + \frac{1}{T} \left(\frac{c_{rms}^*}{c^{*2}} - \frac{[c^* - \bar{c}^*]}{c^* c_{rms}^*} \right) \delta(\mathbf{x} - \mathbf{x}^s), \quad (35)$$

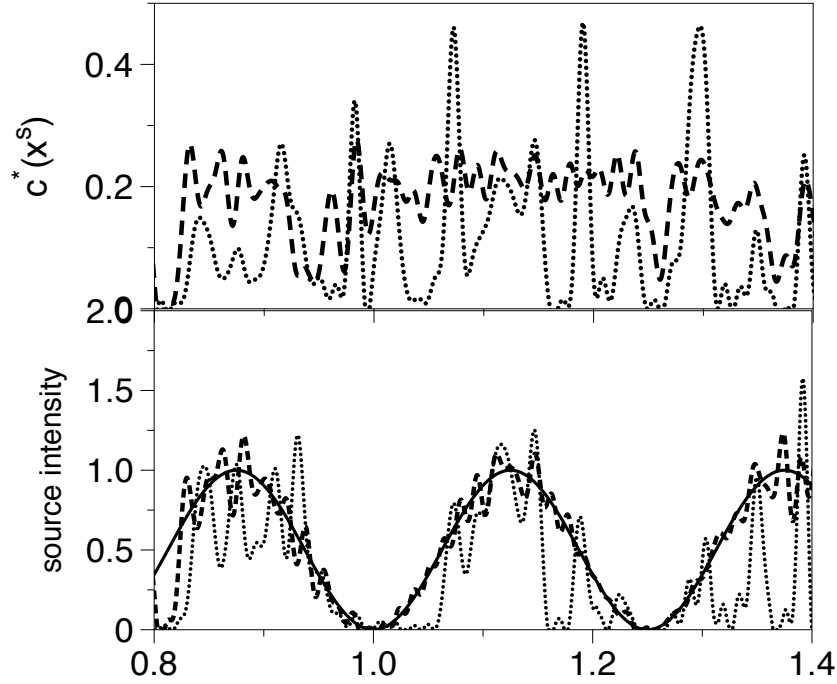


FIG. 13: Comparison of the time traces of (Top) the adjoint field c^* at the source location, and (Bottom) the resultant estimation of scalar source intensity for the initial random trajectory and the optimal trajectory obtained in Case *B2*. Dotted line (.....): initial random trajectory, Dashed line (----): optimal trajectory, Solid line (—): true source intensity.

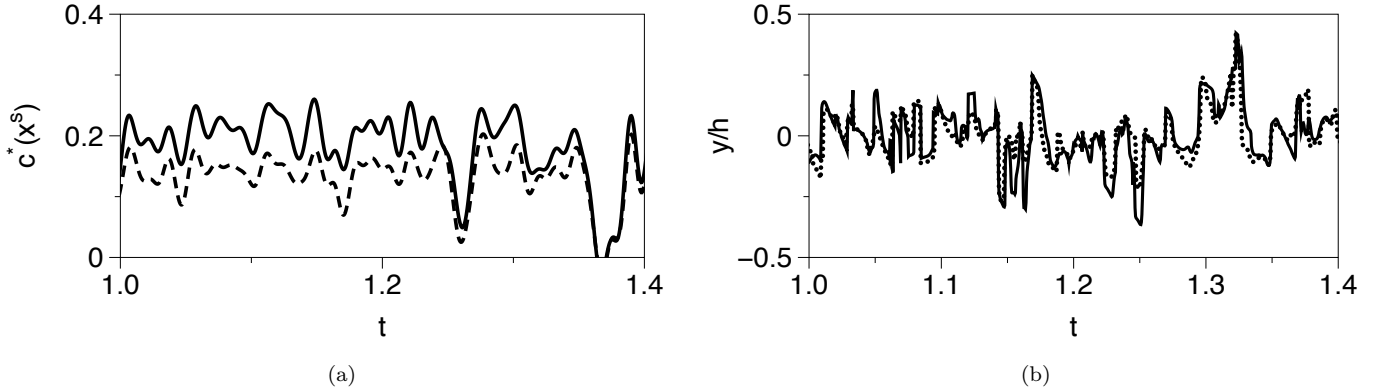


FIG. 14: Comparison between the alternative strategy (----) and the optimal case $R_{21} = 1$ of the initial strategy (—), for a sensor initially at rest at the centerline point. (a) Time trace of the adjoint field at the source location for a limited time horizon. (b) Time trace of the normal coordinate of sensor trajectory.

whereas the formula for updating the sensor trajectory is the same as equation (33). The above equation can be regarded as a modified version of equation (30), in which the weighted coefficients α_1 and α_2 are replaced with the statistics of c^* . As for the initial condition of the sensor trajectory, we consider a stationary sensor located directly downstream of the source. This location was chosen, since it results in the minimum ϵ in the sensing plane when a sensor is stationary.

Figure 14 (a) shows the adjoint fields at the source location for the sensor trajectories optimized by the original cost functional (22) with $(R_{21}, R_{31}) = (1.0, 0)$ (Case *B2*) and the newly introduced cost functional (34). Although the new cost functional yields a slightly lower adjoint field than the original one, the values of ϵ in both cases are similar and around 0.85 after optimization.

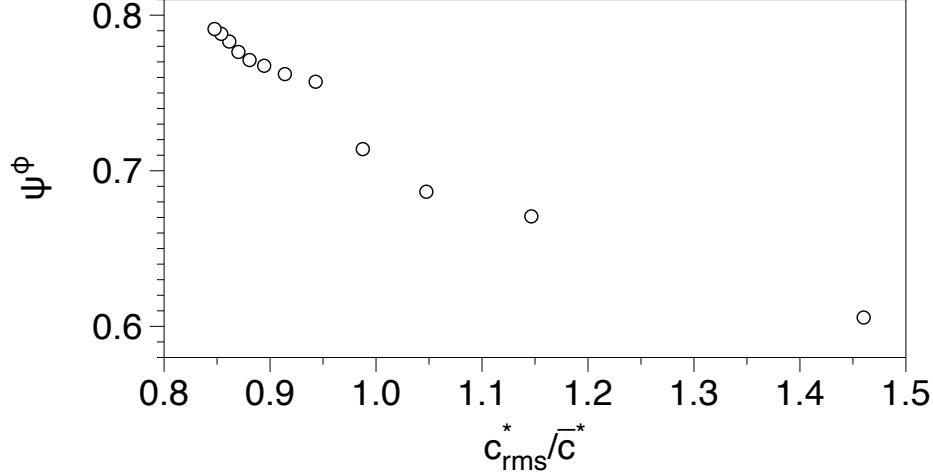


FIG. 15: Correlation coefficient ψ^ϕ as a function of adjoint ratio c_{rms}^*/\bar{c}^* for a mobile sensor whose trajectory is optimized with the new cost functional J_2 . Each open circle refers to a different iteration step of the iterative process.

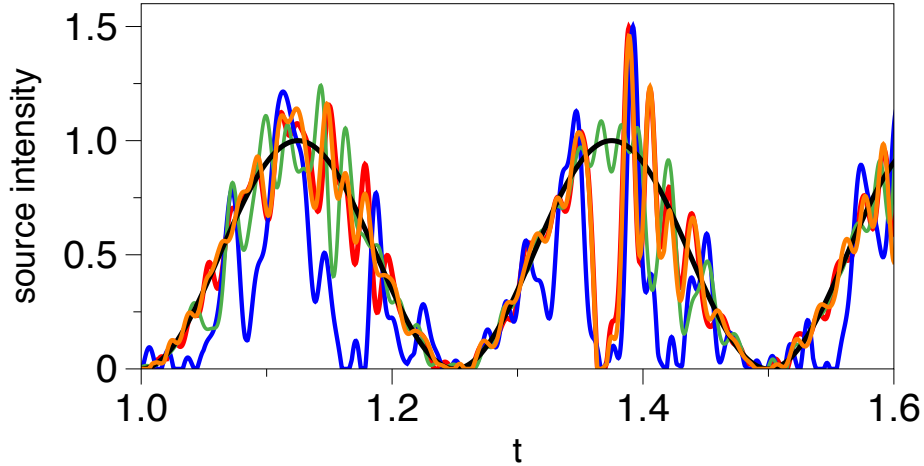


FIG. 16: Time evolution of the reconstructed source profiles for $f = 4$. black: true profile, red: a mobile sensor whose trajectory is optimized with the new cost functional (34), orange: a mobile sensor whose trajectory is optimized with the original cost-functional (case B_2), blue: a single stationary sensor, green: 17 stationary sensors. Only a limited time frame of the entire time horizon is shown.

The time traces of the wall-normal coordinate of the optimal sensor trajectories are compared in figure 14 (b). It is confirmed that the sensor trajectories obtained from the original and new cost functionals are similar. The results shown in figure 14 indicate that the new cost functional (34) without any adjustable parameter is a potential alternative to the original cost functional (22) with the optimal values of R_{21} and R_{31} .

In order to further validate the effectiveness of the new cost functional J_2 , Fig. 15 shows the evolution of the estimation performance, i.e., the correlation coefficient ψ^ϕ between the true and estimated source profiles, as a function of J_2 obtained at every ten iterations in the optimization process. It can be confirmed that the estimation performance is increased with decreasing J_2 .

The time traces of the true and reconstructed source intensity at $f = 4$ are shown in figure 16. The figure includes the estimated source intensities based on a single mobile sensor whose trajectory is optimized by the cost functional J_1 in Case B_2 and the new cost functional J_2 . Also, the estimations with a single and seventeen stationary sensors are plotted for comparison. It can be confirmed that the estimation performance of the single sensor moving along the optimal trajectory obtained by the new cost functional J_2 is as good as that of seventeen stationary sensors.

f	Stationary		Multiple ($n = 17$)		Single Mobile (J_2)	
	Single	ℓ_{norm}^2	ψ^ϕ	ℓ_{norm}^2	ψ^ϕ	ℓ_{norm}^2
2	0.54	0.40	0.96	0.10	0.83	0.22
4	0.60	0.38	0.94	0.13	0.80	0.24
8	0.49	0.41	0.93	0.13	0.84	0.21
16	0.49	0.40	0.93	0.13	0.86	0.20

TABLE II: Comparison of the estimation performances at different source frequencies obtained by a single and seventeen stationary sensors and a single mobile sensor whose trajectory is optimized under the new cost-functional J_2 .

The present optimization strategy is based on the idea to maintain the sensor sensitivity at a source location throughout the entire time horizon. Hence, the resultant optimal trajectory should be effective at different pulsating frequencies. Table II summarizes the estimation quality obtained from a single movable sensor whose trajectory is optimized by the new cost functional (34), and single and multiple stationary sensors at different pulsating frequencies of the source, i.e., $f = 2, 4, 8$ and 16 . We observe that the estimation performance gradually deteriorates with increasing f in all cases. However, the single mobile sensor with the optimal trajectory shows significant improvement compared with the single stationary sensor, and its performance is close to that of seventeen stationary sensors.

VI. SUMMARY AND CONCLUSIONS

In the present study, we consider a problem of scalar source estimation in a turbulent environment. Assuming that the location of a point scalar source is known, the time dependence of the source intensity is estimated based on the signals obtained from a sensor located downstream. Particularly, we focus on developing a new strategy for optimizing a trajectory of a moving sensor.

The key idea behind the present optimization strategy is to maximize the sensor sensitivity and minimize its temporal fluctuation at the source location, whereas the sensor sensitivity is theoretically given by the adjoint scalar field generated at the sensor. Based on this idea, the cost functional (22) is formulated as linear superposition of three different components, i.e., the mean and fluctuating components of the adjoint scalar field, and the penalty of the sensor speed. This naturally yields the extra-adjoint equation based on which the sensor trajectory is iteratively optimized. It is confirmed that the cost functional is monotonically decreased in all cases with increasing number of forward-adjoint iterations, and the sensor trajectories eventually converges to the optimal ones.

The resultant optimal trajectories were implemented to a moving sensor and their performances of scalar source estimation were quantitatively evaluated. It was found that the estimation performance of the single sensor moving along the optimal trajectory is drastically improved from that of a stationary sensor, and almost similar to that of 17 stationary sensors. Systematic optimizations with the different weighting coefficients in the cost functional imply that the ratio ϵ between the fluctuation and the mean of the sensitivity, i.e., the adjoint scalar field at the source location, is a primary factor in deciding the estimation performance. Therefore, we also introduced the new cost functional (34) which includes ϵ only. It was found that the optimal sensor trajectory under the new cost functional yields essentially the same performance as that under the original cost functional with the best combination of the weighting coefficients for the three components. The advantage of the second cost functional is that there is no adjusting parameter. It was also shown that the optimal sensor trajectory is effective in a wide range of the pulsating frequencies.

The present results support that maximizing the sensor sensitivity with less fluctuation is a promising strategy for optimizing a sensor trajectory. It could be easily extended to find the optimal arrangement of stationary sensors and also optimization of the trajectories of multiple moving sensors. In the present study, it is assumed that the location of the scalar source is known. The localization of a steady scalar source with stationary sensors based on the adjoint-based approach is discussed in a recent study [18], and it is interesting to consider how these techniques can be further extended for localizing a scalar source with a moving sensor.

Finally, the present study assumes that the complete information of the spatio-temporal evolution of the velocity field is available. Since this scenario is unrealistic, it is important to take into account the uncertainty of the velocity field and evaluate its impact on the performance of scalar source estimation. Another issue is that the present approach requires iterations of adjoint and extra-adjoint computations, and therefore it is still difficult to apply to on-line optimization of a sensor trajectory in real experiments. Therefore, it is desirable to extract a simple rule of sensor movement based on the local measurements from the obtained optimal sensor trajectory. These issues remain to be addressed in future work.

ACKNOWLEDGMENTS

This study is supported by the Japan Science and Technology Council (JST), Strategic International Collaborative Research Program (SICORP), and by the National Science Foundation (grant CNS1461870)

Appendix A: Derivation of the optimization algorithm

We consider the following cost-functional for optimizing the sensor trajectory:

$$J_1 = -\alpha_1 \int_0^T c^*(\mathbf{x}^s, t) dt + \alpha_2 \int_0^T \left(c^*(\mathbf{x}^s, t) - \bar{c}^*(\mathbf{x}^s) \right)^2 dt + \alpha_3 \int_0^T \mathbf{u}^m \cdot \mathbf{u}^m dt, \quad (\text{A1})$$

where α_i represent relative importance of each term. The perturbation of the Hamiltonian function H due to the small change of the sensor trajectory \mathbf{x}^m is written as

$$H' = J'_1 + \left\langle \theta \left\{ \frac{\partial c^{*'}}{\partial t^*} - u_j \frac{\partial c^{*'}}{\partial x_j} - \frac{1}{Pe} \frac{\partial^2 c^{*'}}{\partial x_j^2} - \frac{\partial \delta(x_j - x_j^m)}{\partial x_j^m} x_j^{m'} \right\} \right\rangle. \quad (\text{A2})$$

The first term of the above equation arises from the perturbation of the cost-functional, denoted as H'_a , can be written as

$$H'_a = J'_1 = \langle c^{*'} \left\{ -\alpha_1 + 2\alpha_2 \left[c^* - \bar{c}^* \right] \right\} \delta(\mathbf{x} - \mathbf{x}_s) \rangle + \int_0^T H'_{\mathcal{B},2} dt + \int_0^T H'_{\mathcal{B},2} x_j^{m'} dt, \quad (\text{A3})$$

where we introduce the following identities :

$$H'_{\mathcal{B},2} = \frac{d}{dt} \left[2\alpha_3 x_j^{m'} \frac{dx_j^m}{dt} \right], \quad (\text{A4a})$$

$$H'_{\mathcal{B},2} = -2\alpha_3 \frac{d^2 x_j^m}{dt^2}. \quad (\text{A4b})$$

The remaining part of eq. (A2), denoted as H'_b , can be written as

$$H'_b = H' - H'_a = \left\langle c^{*'} \left[-\frac{\partial \theta}{\partial t^*} + \frac{\partial(\theta u_j)}{\partial x_j} - \left\{ \frac{\partial}{\partial x_j} \left(\frac{1}{Pe} \frac{\partial \theta}{\partial x_j} \right) \right\} - \frac{\partial \theta}{\partial x_j} \delta(x_j - x_j^m) x_j^{m'} \right] \right\rangle + \mathcal{B}, \quad (\text{A5})$$

where

$$\mathcal{B} = \left\langle \frac{\partial \theta c^{*'}}{\partial t^*} + \frac{\partial}{\partial x_j} \left\{ -\theta c^{*'} u_j + \frac{1}{Pe} c^{*'} \frac{\partial \theta}{\partial x_j} - \frac{1}{Pe} \theta \frac{\partial c^{*'}}{\partial x_j} + \theta \delta(x_j - x_j^m) \right\} \right\rangle. \quad (\text{A6})$$

Substituting eqs. (A3), (A5) into (A2) and introducing a new time coordinate $t^* = T - t$ yield the following expression:

$$H' = \langle c^{*'} \left[\frac{\partial \theta}{\partial t} + \frac{\partial(\theta u_j)}{\partial x_j} - \left\{ \frac{\partial}{\partial x_j} \left(\frac{1}{Pe} \frac{\partial \theta}{\partial x_j} \right) \right\} + \left\{ -\alpha_1 + 2\alpha_2 \left[c^* - \bar{c}^* \right] \right\} \delta(\mathbf{x} - \mathbf{x}^s) \right] \rangle - \left\langle \frac{\partial \theta}{\partial x_j} \delta(x_j - x_j^m) x_j^{m'} \right\rangle - 2\alpha_3 \int \frac{d^2 x_j^m}{dt^2} x_j^{m'} dt + \mathcal{B}^*, \quad (\text{A7})$$

where the boundary term \mathcal{B}^* is given by

$$\mathcal{B}^* = \mathcal{B} + 2\alpha_3 \int_0^T \frac{d}{dt} \left[x_j^{m'} \frac{dx_j^m}{dt} \right]. \quad (\text{A8})$$

In order to remove the first term on the right-hand-side of Eq. (A7), we impose the following equation for θ :

$$\frac{\partial \theta}{\partial t} + \frac{\partial(\theta u_j)}{\partial x_j} = \left\{ \frac{\partial}{\partial x_j} \left(\frac{1}{Pe} \frac{\partial \theta}{\partial x_j} \right) \right\} + \left\{ \alpha_1 - 2\alpha_2 \left[c^* - \bar{c}^* \right] \right\} \delta(\mathbf{x} - \mathbf{x}^s), \quad (\text{A9})$$

which describes the spatial and temporal evolution of θ . We further assume that the above equation is accompanied with the following set of boundary conditions:

$$\theta(\mathbf{x}, t = 0) = 0, \quad \frac{\partial \theta}{\partial x_j} n_j = 0, \quad \text{at } \partial \Omega. \quad (\text{A10})$$

so that the boundary term B^* becomes zero. Substituting Eqs. (A9), (A10) into Eq. (A7) results in

$$\begin{aligned} H' &= \left\langle -\frac{\partial\theta}{\partial x_j} \delta(x_j - x_j^m) x_j^{m'} \right\rangle - 2\alpha_3 \int \frac{d^2 x_j^m}{dt^2} x_j^{m'} dt \\ &= \int_0^T - \left[\left(\frac{\partial\theta}{\partial x_j} \right)_{\mathbf{x}^m} + 2\alpha_3 \frac{d^2 x_j^m}{dt^2} \right] x_j^{m'} dt. \end{aligned} \quad (\text{A11})$$

Equation (A11) indicates that H' is always negative by updating the sensor trajectory based on the following formula:

$$x_j^{m'}(t) \left(\equiv x_j^{m,n+1}(t) - x_j^{m,n}(t) \right) = \alpha^n \left[\left(\frac{\partial\theta}{\partial x_j} \right)_{\mathbf{x}^m} + 2\alpha_3 \frac{d^2 x_j^m}{dt^2} \right]^n, \quad (\text{A12})$$

where the second superscript of n indicates a iteration step and α^n is a positive coefficient determining the amount of the update in the n -th iteration step.

Appendix B: Derivation of optimization algorithm for the cost-functional J_2

We seek to find the optimal sensor trajectory to minimize the following cost functional:

$$J_2 = \frac{c_{rms}^*(\mathbf{x}^s)}{c^*(\mathbf{x}^s)} = \frac{\left\{ \frac{1}{T} \int_0^T [c^* - \bar{c}^*]^2 \delta(\mathbf{x} - \mathbf{x}^s) dt \right\}^{1/2}}{\frac{1}{T} \int_0^T c^* \delta(\mathbf{x} - \mathbf{x}^s) dt}. \quad (\text{B1})$$

For convenience, we introduce the following identities:

$$\begin{aligned} w &= c_{rms}^*(\mathbf{x}^s) = \left\{ \frac{1}{T} \int_0^T [c^* - \bar{c}^*]^2 \delta(\mathbf{x} - \mathbf{x}^s) dt \right\}^{1/2}, \\ g &= \overline{c^*(\mathbf{x}^s)} = \frac{1}{T} \int_0^T c^* \delta(\mathbf{x} - \mathbf{x}^s) dt. \end{aligned} \quad (\text{B2})$$

The perturbations of w and g with respect to the sensor location \mathbf{x}^m are respectively given by

$$\begin{aligned} w' &= \frac{\langle c^{*'} [c^* - \bar{c}^*] \delta(\mathbf{x} - \mathbf{x}^s) \rangle}{T c_{rms}^*}, \\ g' &= \frac{1}{T} \langle c^{*'} \delta(\mathbf{x} - \mathbf{x}^s) \rangle. \end{aligned} \quad (\text{B3})$$

The perturbation of the cost functional (B1) can be obtained by applying the quotient rule as follows:

$$J_2' = \left[\frac{g w' - w g'}{g^2} \right] = \frac{1}{T} \langle c^{*'} \left\{ \frac{[c^* - \bar{c}^*]}{c^* c_{rms}^*} - \frac{c_{rms}^*}{c^{*2}} \right\} \delta(\mathbf{x} - \mathbf{x}^s) \rangle. \quad (\text{B4})$$

Applying the same procedure as described in Appendix A to Eq. ((B4)) leads to the following partial differential equation for θ :

$$\frac{\partial\theta}{\partial t} + \frac{\partial(\theta u_j)}{\partial x_j} = \left\{ \frac{\partial}{\partial x_j} \left(\frac{1}{Pe} \frac{\partial\theta}{\partial x_j} \right) \right\} + \left\{ \frac{c_{rms}^*}{c^{*2}} - \frac{[c^* - \bar{c}^*]}{c^* c_{rms}^*} \right\} \delta(\mathbf{x} - \mathbf{x}^s). \quad (\text{B5})$$

The boundary conditions and the iterative expression for \mathbf{x}^m remain the same as those shown in Eqs. (A10) and (A12), respectively.

-
- [1] G. Kowadlo and R. Russell, Robot odor localization: A taxonomy and survey., *Int. J. Robot. Res.* **27(8)**, 869 (2008).
- [2] H. Ishida, Y. Wada, and H. Matsukura, Chemical sensing in robotic applications: A review., *IEEE Sens. J.* **12**, 3163 (2012).
- [3] S. Kennedy and D. Marsh, Pheromone-regulated anemotaxis in flying moths., *Science* 184.4140 **184**, 999 (1974).
- [4] M. Muller and R. Wehner, The hidden spiral: systematic search and path integration in desert ants, *cataglyphis fortis.*, *J. Comp. Physiol. A* **175**, 525530 (1994).
- [5] D. Harvey, T. Lu, and M. Keller, Comparing insect-inspired chemical plume tracking algorithms using a mobile robot., *IEEE. T. Robot.* **24(2)**, 307 (2008).
- [6] N. Voges, A. Chaffiol, P. Lucas, and D. Martinez, Reactive searching and infotaxis in odor source localization., *PLoS Comput. Biol.* **10(10)**, e1003,861 (2014).
- [7] M. Patan and K. Patan, Optimal observation strategies for model-based fault detection in distributed systems., *Int. J. Control* **78:18**, 1497 (2005).
- [8] J. Pudykiewicz, Application of adjoint tracer transport equations for evaluating source parameters., *Atmos. Environ.* **32**, 3039 (1998).
- [9] M. Sohn, P. Reynolds, N. Singh, and A. Gadgil, Rapidly locating and characterizing pollutant releases in buildings., *J. Air Waste Manage.* **52**, 1422 (2002).
- [10] D. Ucinski, Optimal sensor location for parameter estimation of distributed processes., *Int. J. Control* **73:13**, 1235 (2000).
- [11] V. Mons, Q. Wang, and T. Zaki, Kriging-enhanced ensemble variational data assimilation for scalar-source identification in turbulent environments, *J. Comp. Phys.* **398**, 108856 1 (2021).
- [12] T. Bewley, P. Moin, and R. Temam, Dns-based predictive control of turbulence: an optimal benchmark for feedback algorithms., *J. Fluid Mech.* **447**, 179 (2001).
- [13] D. Ucinski and P. Baranowski, A parallel algorithm for optimum monitoring network design in parameter estimation of distributed systems., in *Proceedings of the European Control Conference (ECC), Zurich, Switzerland, July 17-19* (2013).
- [14] M. Wang, Q. Wang, and T. A. Zaki, Discrete adjoint of fractional-step incompressible navier-stokes solver in curvilinear coordinates and application to data assimilation, *Journal of Computational Physics* **396**, 427 (2019).
- [15] M. Vergassola, E. Villermaux, and B. Shraiman, "infotaxis" as a strategy for searching without gradients., *Nature* **445(7126)**, 406 (2007).
- [16] A. Keats, E. Yee, and F.-S. Lien, Bayesian inference for source determination with applications to a complex urban environment., *Atmos. Environ.* **41(3)**, 465 (2007).
- [17] D. Cerizza, W. Sekiguchi, T. Tsukahara, T. Zaki, and Y. Hasegawa, Reconstruction of scalar source intensity based on sensor signal in turbulent channel flow., *Flow. Turbul. Combust.* **97**, 1211 (2016).
- [18] Q. Wang, Y. Hasegawa, and T. A. Zaki, Spatial reconstruction of steady scalar sources from remote measurements in turbulent flow, *J. Fluid Mech.* **870**, 316 (2019).
- [19] N. Baker and N. Daley, Observation and background adjoint sensitivity in the adaptive observation-targeting problem., *Q. J. R. Meteorol. Soc.* **126**, 1431 (2000).
- [20] R. Langland and N. Baker, Estimation of observation impact using the nrl atmospheric variational data assimilation adjoint system., *Tellus* **56A**, 189 (2004).
- [21] D. Daescu, On the sensitivity equations of four-dimensional variational (4d-var) data assimilation., *Mon. Weather Rev.* **136(8)**, 3050 (2008).
- [22] T. Misaka and S. Obayashi, Sensitivity analysis of unsteady flow fields and impact of measurement strategy., *Math. Probl. Eng.* , 1 (2014).
- [23] W. Kang and L. Xu, Optimal placement of mobile sensors for data assimilations., *Tellus A: Dynamic Meteorology and Oceanography* **64**, 17133 1 (2012).
- [24] A. Krener and K. Ide, Measures of unobservability, *Joing 48th IEE Conference on Decision and Control and 28th Chinese Control Conference* **126**, 6401 (2009).
- [25] V. Mons, J. Chassaing, and P. Sagaut, Optimal sensor placement for variational data assimilation of unsteady flow past a rotationally oscillating cylinder, *J. Fluid Mech.* **823**, 230 (2017).
- [26] D. Ucinski and Y. Chen, Sensor motion planning in distributed parameter systems using turing's measure of conditioning., in *Proceedings of the 45th IEEE Conference on Decision & Control, San Diego, USA, December 13-15* (2006).
- [27] C. Tricaud and Y. Chen, Optimal trajectories of mobile remote sensors for parameter estimation in distributed cyber-physical systems. (American Control Conference, Baltimore, USA, 2010) pp. 3211–3215.
- [28] S. Verma, C. Papadimitriou, N. Luethen, G. Arampatzis, and P. Koumoutsakos, Optimal sensor placement for artificial swimmers, *J. Fluid Mech.* **884**, A24 1 (2020).
- [29] Z. Deng, C. He, and Y. Liu, Deep neural network-based strategy for optimal sensor placement in data assimilation of turbulent flow, *Phys. Fluids* **33**, 025119 1 (2021).
- [30] Y. Hasegawa and N. Kasagi, Dissimilar control of momentum and heat transfer in a fully developed turbulent channel flow., *J. Fluid Mech.* **683**, 57 (2011).
- [31] T. Suzuki and Y. Hasegawa, Estimation of turbulent channel flow at $re_\tau = 100$ based on the wall measurement using a simple sequential approach, *J. Fluid Mech.* **830**, 760 (2017).